

Residual landslide susceptibility analysis based on integrated machine learning framework

Shou Hao, Chiang, Tung Cheng, Lu

First Author's Affiliation: Professor, Center for Space and Remote Sensing Research, National Central University, Taiwan

Second Author's Affiliation: Research Assistant, Center for Space and Remote Sensing Research, National Central University, Taiwan

thomsonlu1028@gmail.com

Abstract: *In this study, residual landslides refer to slopes characterized by substantial accumulations of landslide-derived failure materials, forming unstable colluvium that may serve as primary source zones for debris flows, especially under conditions of intense rainfall, thereby posing significant hazards to downstream areas. In Taiwan, such residual landslides present a critical challenge for watershed management and sediment-related disaster mitigation. The inaccessibility of mountainous terrain, combined with the increasing frequency and intensity of extreme precipitation events driven by climate change, has exacerbated the risks and unpredictability associated with landslides and debris flows. To address these challenges, this study proposes an advanced machine learning framework for assessing residual landslide hazards. The approach involves the development of a predictive model to evaluate the potential activity of residual landslides through the integration of temporal remote sensing data, including time-series satellite observations from Sentinel-1 and Sentinel-2. This methodology enables systematic inventory mapping and activity assessment across mountainous regions, thereby enhancing early warning capabilities and informing more effective sediment disaster prevention and management strategies.*

Keywords: *Residual landslide, Sentinel-1, Sentinel-2, machine learning, Taiwan*

Introduction

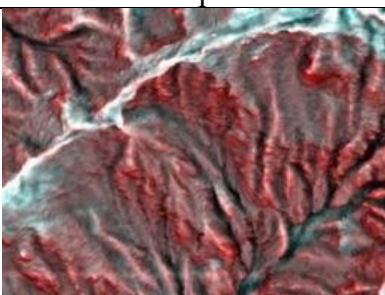
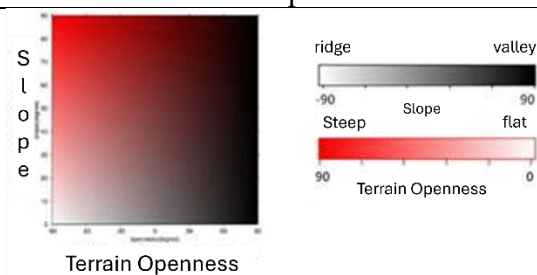
In Taiwan, the frequent occurrence of typhoons and earthquakes has made landslides a prevalent geological and sediment-related hazard in mountainous regions. Slopes with substantial accumulations of unstable debris often serve as primary sources of debris flows during extreme rainfall events, posing significant threats to downstream areas and presenting a critical challenge for watershed management. These risks are further exacerbated by the remoteness and inaccessibility of many mountainous terrains, as well as by the intensification of extreme precipitation under climate change. To enhance risk monitoring and disaster preparedness, the Department of Rural Development and Soil and Water Conservation (ARDSWC) has conducted comprehensive surveys of slopes across Taiwan and has introduced two key classifications of debris flow sources: “residual landslide” and “unstable debris.” The term residual landslide denotes slope surfaces where bedrock is exposed, or residual sediments are deposited as a result of natural landslides or similar processes. Unstable debris refers to large sediment accumulations on these residual


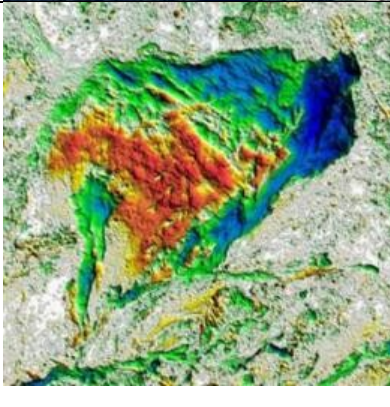
landslides or within river channels that exist in a transient or unstable state of equilibrium. When triggered by rainfall, earthquakes, or other external forces, these sediments can be mobilized and subsequently generate severe hazards in downstream regions.

According to the *Residual landslide Identification Manual* published by the Department of Rural Development and Soil and Water Conservation (ARDSWC) in 2024, the interpretation process for residual landslide sediments is divided into five major steps:

1. **Preliminary identification of residual landslide sites:** Multi-temporal high-resolution satellite imagery from Google Earth Pro and its 3D terrain visualization platform are used to observe topographic changes. Reference is made to five common morphological features of residual landslides—head scarp, landslide depression scarp, twin gullies with the same origin, displaced landforms, and talus accumulation—to mark potential residual landslide sites.
2. **Secondary verification of residual landslide sites:** Multi-temporal satellite imagery from Google Earth and the H.O.S.T. map are employed to confirm residual landslide features. In addition, airborne LiDAR-derived DEMs of Difference (DoD) are utilized to assess the activity of residual landslide sediments (Table 1).
3. **Image Clipping:** After selecting the landslide-prone units of interest, the three auxiliary interpretation image datasets used for the validation points (Google Earth multi-temporal satellite imagery, H.O.S.T maps, and airborne LiDAR-based Digital Elevation Model change detection maps (DoD)) were clipped using the polygon tool in Google Earth.

Table 1: Ancillary Imagery for Residual Slope Interpretation

Tool	Graphic	Description
H.O.S.T.map		

Multi-temporal satellite imagery		Observe the changes in sediment movement by examining the series of images generated chronologically within the KML file produced by the system
Airborne LiDAR Digital Terrain Difference Analysis Map (DEM of Difference map, DoD map)		The results of subtracting two-period LiDAR DEM data show that the red and yellow color schemes may indicate a phenomenon of deposition (where the terrain changes from low to high), while the blue and green color schemes may indicate erosion (where the terrain changes from high to low).

4. **Image clipping:** After selecting residual landslide units within the study area, the polygon tool in Google Earth is applied to clip the three auxiliary interpretation datasets used in verification—Google Earth multi-temporal imagery, H.O.S.T. maps, and LiDAR-based DoD maps.
5. **Digitization of residual landslide features:** The clipped imagery of residual landslide units is digitized in Google Earth based on the geometric characteristics defined in the residual landslide morphological feature table.

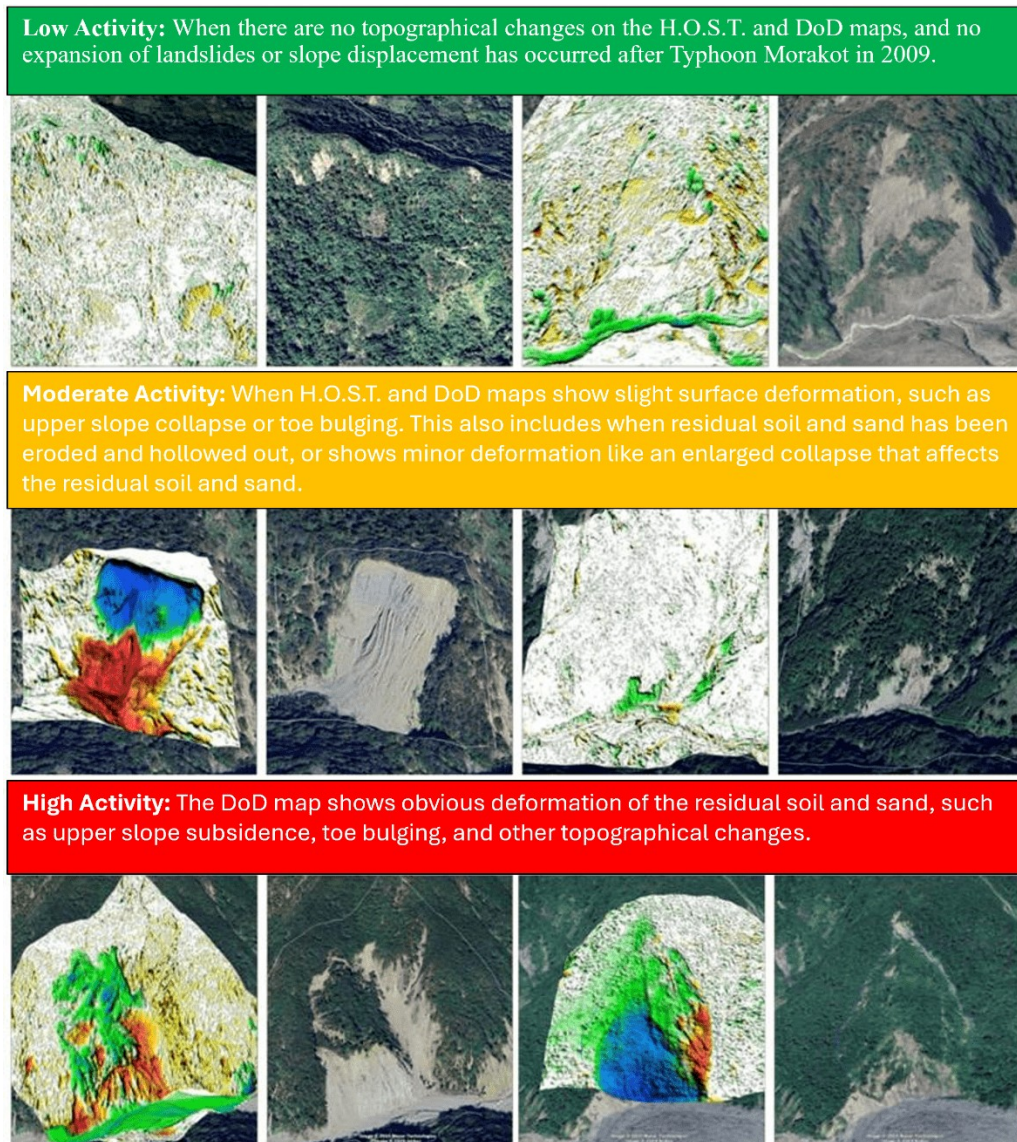


Figure 1: Example of Residual Soil and Sand Activity Assessment Method

6. **Interpretation of activity and risk levels:** Residual landslide activity is assessed by comparing multi-temporal H.O.S.T. maps, DoD layers, and satellite images. The degree of change over time is categorized into three levels:

- *Low activity:* No detectable changes in H.O.S.T. maps or DoD layers, and no evidence of landslide expansion or slope displacement after Typhoon Morakot (2009).
- *Moderate activity:* Minor surface deformation detected in H.O.S.T. maps or DoD layers, such as head scarp subsidence, toe bulging, erosion at the slope foot, or slight deformation/expansion of residual landslide sediments.
- *High activity:* Significant deformation of residual landslide sediments observed in DoD layers, including pronounced head scarp subsidence or

toe bulging.

The corresponding interpretation criteria are illustrated in Figure 1.

Based on the 2024 SWCA nationwide survey, a total of 556 residual landslide sites (comprising 747 individual slope units) have been identified across Taiwan. Among these, the Gaoping River Basin accounts for the largest proportion, with 117 sites (229 units), highlighting the region as a high-risk area for sediment-related disasters. In light of this, the present study aims to develop an artificial intelligence–based analytical framework for assessing the potential of residual landslides.

Literature Review

Section 1. Overview of Environmental Data

The Gaoping River Basin is primarily composed of tributaries such as the Laonong River, Nanzixian River, and Ailiao River, all originating from the Central Mountain Range near Yushan. The upstream region, located in the northeastern part of the basin, is characterized by higher elevations and steep terrain dominated by mountainous landscapes. In contrast, the downstream area in the southwest features lower elevations and gentler slopes, transitioning into plains.

According to the 2024 residual landslide inventory conducted by the Soil and Water Conservation Agency (SWCA), residual landslides within the Gaoping River Basin are mainly concentrated in the mid- to upstream regions. This spatial distribution pattern aligns closely with the *Potential Zonation Map of Unstable Sediment Watersheds* released by the SWCA, indicating that most residual landslides are situated within at least medium-to-high potential unstable sediment watersheds (Figure 2). By overlaying the basin boundaries, the unstable sediment potential zonation, and the residual landslide distribution, an experimental area was delineated in accordance with the objectives of this study. The experimental area covers approximately 2,241 km², with elevation ranging from 92 to 3,944 m, slopes ranging from 0 to 86.4°, and an average slope of 34.6°.

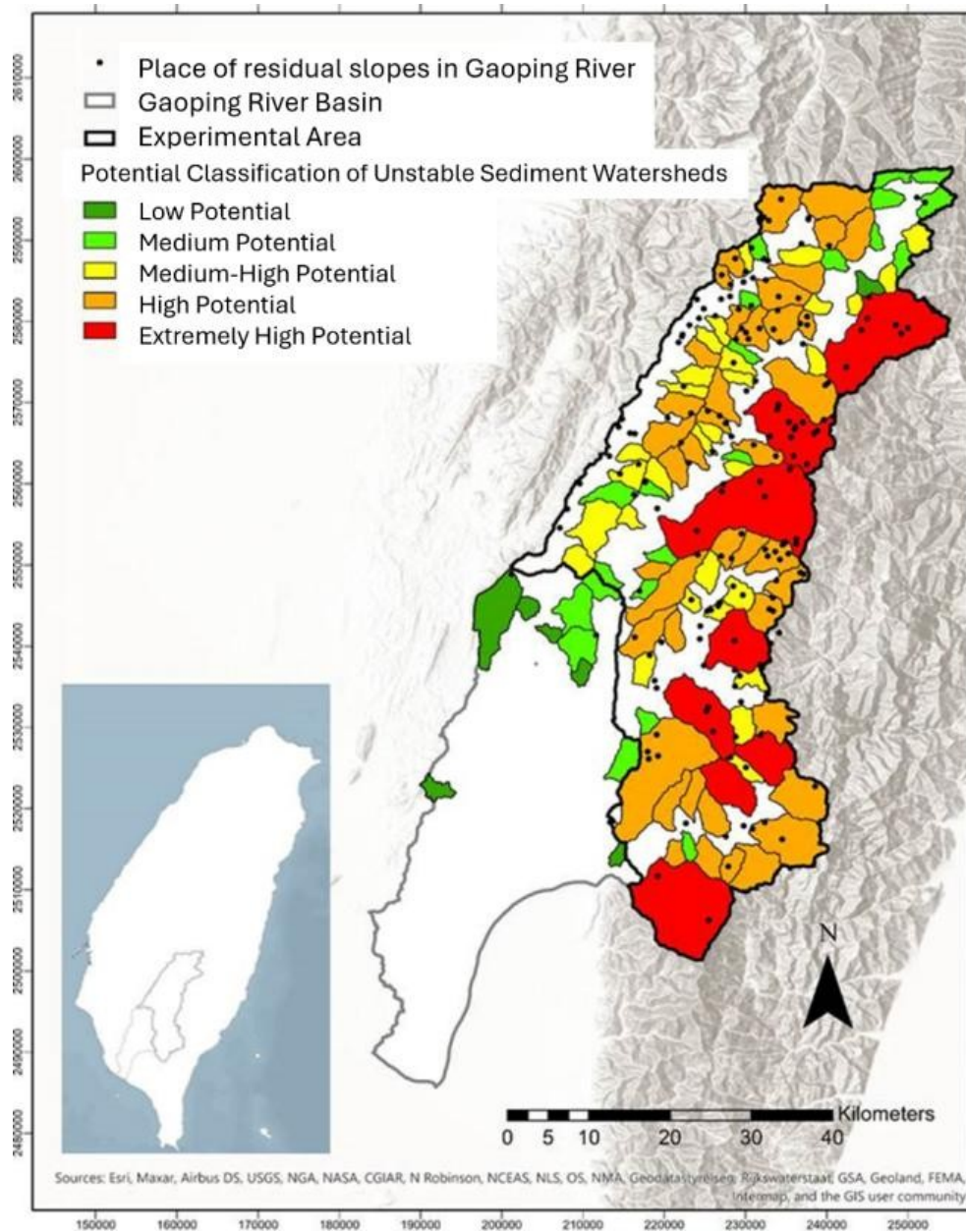


Figure 2: Distribution of unstable sediment watershed potential zones and residual landslides in the Gaoping River Basin

The lithology of the Gaoping River Basin consists primarily of Paleozoic to Mesozoic black and green schists; Eocene to Oligocene slates and quartzites; Miocene to Pliocene sandstones and shales; Pleistocene fluvial deposits; and Cenozoic alluvium. Climatically, the basin exhibits distinct wet and dry seasons, with an average annual rainfall of approximately 2,454 mm. Between May and October, the influence of the southwest monsoon and frequent typhoon events accounts for nearly 82% of the total annual precipitation. Spatially, precipitation is significantly higher near the Central Mountain Range, whereas rainfall in the lowland and coastal areas is comparatively lower.

Section 2. Historical Landslides

This study analyzes event-based landslide records from the *BigGIS Spatial Information System* maintained by the Ministry of Agriculture, Soil and Water Conservation Agency (<https://gis.ardswc.gov.tw/>), which documents the spatial distribution and affected area of landslides for each year. The minimum mapping unit for landslide events in this dataset is 0.1 ha. To construct a dataset of historical landslide events within the experimental area, all events fully contained within the study boundaries were extracted and exported annually, including both event counts and landslide-affected areas.

To further enrich the dataset, major disaster reports published on the Debris Flow Disaster Prevention Information Network were referenced. Beginning from 2008, the names and numbers of major sediment-related disasters occurring within the experimental area were compiled for each year through 2024 (Table 2). The results reveal interannual variability in the number of recorded landslides. For example, Typhoon Morakot in 2009 triggered a particularly severe impact, resulting in 3,856 landslide events. In contrast, no landslides were recorded in 2022 (Figure 3).

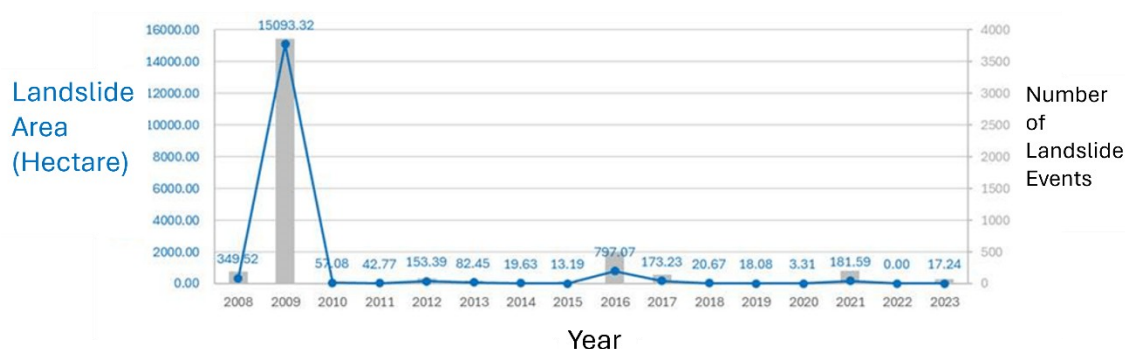


Figure 3: Annual number and area of landslide events in the experimental area

Table 2: Disaster inventory and number of major sediment-related disaster events in the experimental area

Year	Event	Date	Severe Cases	Year	Event	Date	Severe Cases
2008	Talim Typhoon	07/17	13	2015	May 20 Heavy Rain	05/20	0
	Phanfone Typhoon	07/28	0		Lotus Typhoon	07/08	0
	Sinlaku Typhoon	09/14	0		Chan-hom Typhoon	07/10	0
	Charming Typhoon	09/22	0		Soudelor Typhoon	08/08	0
2009	Morakot Typhoon	08/08	41		Swallow Typhoon	08/23	0
	Baema Typhoon	10/05	0		Dujuan Typhoon	09/28	0
	Oct 11 Heavy Rain	10/11	0	2016	June 10 Heavy Rain	06/10	1
2010	July 26 Heavy Rain	07/26	0		June 29 Heavy Rain	06/29	0
	Nam Sio Typhoon	08/31	0		Nepartak Typhoon	07/08	0
	Lionrock Typhoon	09/01	0		July 10 Heavy Rain	07/10	0
	Moranti Typhoon	09/09	0		Moranti Typhoon	09/14	0
	Fanapi Typhoon	09/19	1		Malakas Typhoon	09/17	0
	Sept 24 Heavy Rain	09/24	0		Meggi Typhoon	09/27	1
	Oct 16 Heavy Rain	10/16	0		Eli Typhoon	10/06	0
	Oct 17 Heavy Rain	10/17	0		Oct 12 Heavy Rain	10/12	0
	Meggi Typhoon	10/22	0	2017	June 01 Heavy Rain	06/01	1
2011	July 19 Heavy Rain	07/19	0		June 13 Heavy Rain	06/13	0
	South Madhu Typhoon	08/29	0		Nesat Typhoon	07/29	0
	Oct 01 Heavy Rain	10/01	0		Aug 01 Heavy Rain	08/01	0
	Nov 17 Heavy Rain	11/17	0	2018	Aug 23 Low Pressure	08/23	1
2012	May 12 Heavy Rain	05/12	0	2019	May 18 Heavy Rain	05/18	0
	May 20 Heavy Rain	05/20	0		June 11 Heavy Rain	06/11	0
	June 10 Heavy Rain	06/10	2		Other	06/27	1
	Talim Typhoon	06/20	0		Danas Typhoon	07/18	0
	Soulik Typhoon	08/02	0		Lekima Typhoon	08/11	1
	Fitow Typhoon	08/24	0		Aug 15 Heavy Rain	08/15	2
	Fitow Typhoon	08/28	0		Bailu Typhoon	08/24	0
	Sept 15 Heavy Rain	09/15	0	2020	May 21 Heavy Rain	05/21	0
	Jelawat Typhoon	09/28	0		May 28 Heavy Rain	05/28	0
	May 17 Heavy Rain	05/17	0	2021	Caiyun Typhoon	06/04	0
2013	Soulik Typhoon	07/13	1		June 21 Heavy Rain	06/21	0
	Tammy Typhoon	08/21	0		July 31 Heavy Rain	07/31	0
	Kong-rey Typhoon	08/29	0		Lupit Typhoon	08/07	3
	Danielle Typhoon	09/21	0	2023	Kanu Typhoon	08/04	0
	Fitow Typhoon	10/06	0		Other	08/23	1
2014	May 20 Heavy Rain	05/20	0		Haikui Typhoon	09/03	0
	June 06 Heavy Rain	06/06	0		Kujira Typhoon	10/05	1
	Megdhom Typhoon	07/23	0	2024	Kammuri Typhoon	07/25	4
	Phanfone Typhoon	09/21	0		Other	09/22	1

Section 3. Residual landslides within the Experimental Area

Based on the 2024 residual landslide inventory by the SWCA, data are organized around point-based attributes combined with vector datasets, comprehensively recording the details of each residual landslide. The information can be categorized into four major groups:

1. Geographic attributes

- *Residual landslide centroid*: The central location of the slope.
- *Associated watershed and ID*: The watershed unit and its identification code.
- *Sediment extent*: The residual landslide sediment area delineated using polygon vector data.

2. Morphological attributes

- *Topographic features*: Types and counts of morphological features represented as polylines or polygons, including head scarps, depression scarps, twin gullies, displaced landforms, and talus accumulations (six types in total).
- *Slope length and displacement*: Line features recording slope length and measured displacement over time.
- *Estimated sediment volume*: Including both areal extent and estimated volume of sediment cover.

3. Activity-related attributes

- *Activity level*: Expert interpretation of slope activity.
- *Basis of interpretation*: Supporting datasets referenced in determining activity levels (as illustrated in Figure 1).
- *Imagery source*: The most recent imagery used during interpretation.

4. Risk-related attributes

- *Risk level*: Overall hazard risk classification.
- *Basis of risk assessment*: Derived from both activity levels and proximity to protected objects.
- *Protection objects*: Names and straight-line distances of the nearest protection targets.

Within the experimental area, a total of 168 residual landslides were identified, with activity levels distributed as follows: 71 low-activity, 67 moderate-activity, and 30 high-activity sites (Figure 4). Among morphological types, head scarps are the most prevalent, accounting for 76% of all identified residual landslides.

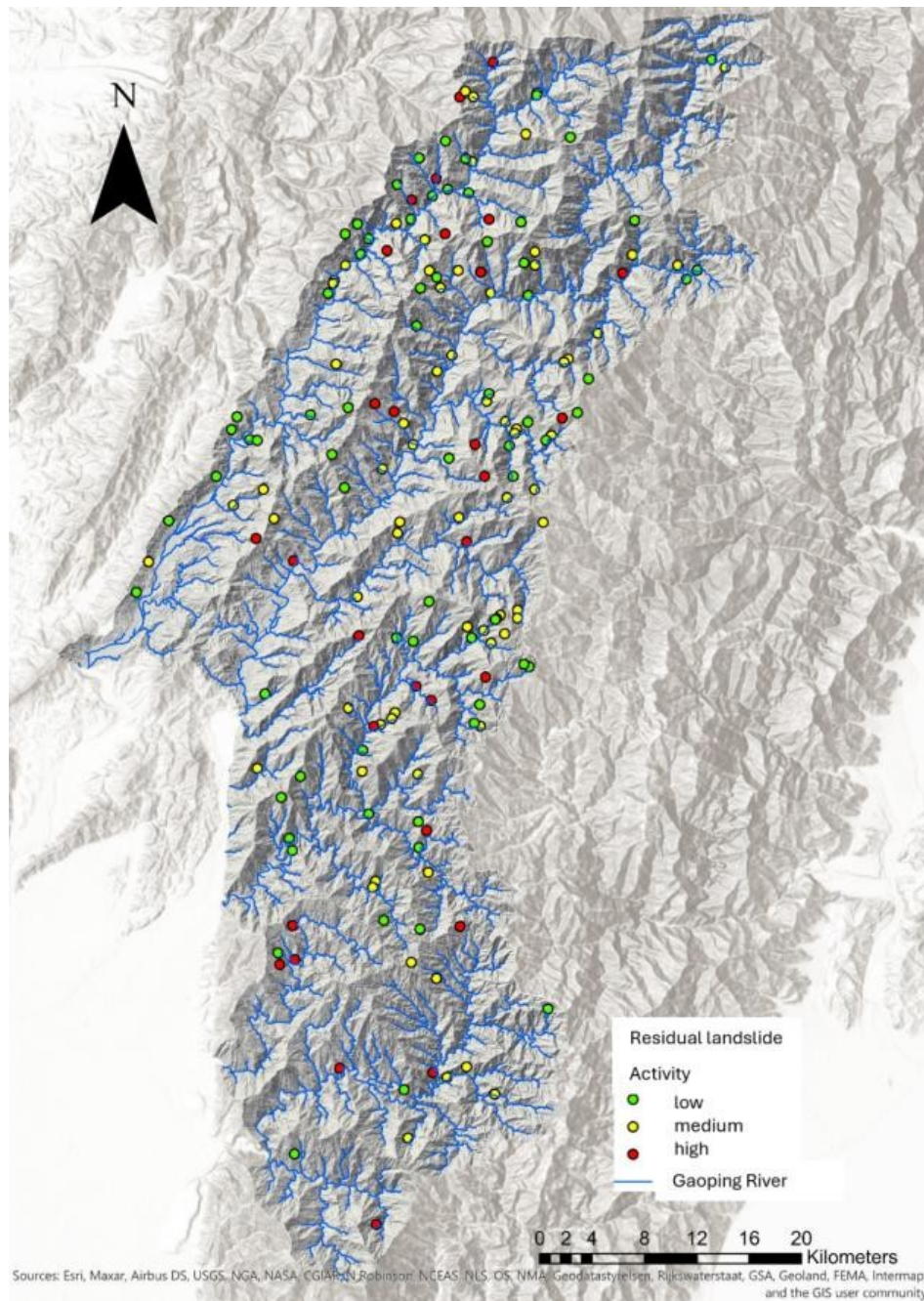


Figure 4: Distribution of residual landslide activity levels in the experimental area

Methodology

The primary objective of this study is to develop a CNN–Transformer-based model for residual landslide potential analysis, using the Gaoping River Basin as the experimental area. The model aims to classify slope potential levels based on activity (low, moderate, and high). Model training integrates multiple datasets, including satellite imagery, geomorphology, soil, geology, and rainfall data, with particular emphasis on multi-temporal satellite imagery (e.g., Sentinel-1 and Sentinel-2).

Section 1. Model Description

This study proposes an artificial intelligence model that integrates Convolutional Neural Networks (CNNs) and Transformer architectures. CNNs are effective in extracting multiple spatial features from imagery for model training, whereas Transformers—originating from large-scale language models—introduce a self-attention mechanism that enables efficient parameterization of sequential data. Due to their ability to handle parallel computation, Transformers significantly accelerate training speed and are particularly well-suited for multi-temporal imagery, capturing the dynamic evolution of residual landslides.

The integration of CNN and Transformer architectures requires careful consideration of training data, input characteristics, and appropriate loss function design. Hyperparameters such as batch size and learning rate are tuned, and multiple network structures are tested to optimize model performance.

(a) Convolutional Neural Network (CNN)

CNNs (Figure 5) are deep learning models designed for structured data, particularly imagery. In landslide modeling, CNNs have been widely applied for feature extraction (Zhao and Cai, 2017). Their basic structure includes:

- **Input Layer:** Image pixel matrices or other structured data.
- **Convolutional Layer:** Feature extraction using filters through convolution operations.
- **Pooling Layer:** Max pooling or average pooling to reduce feature map size while retaining essential information.
- **Fully Connected Layer:** Flattening extracted features for classification or regression tasks.
- **Output Layer:** Producing final classification results via activation functions such as Softmax.

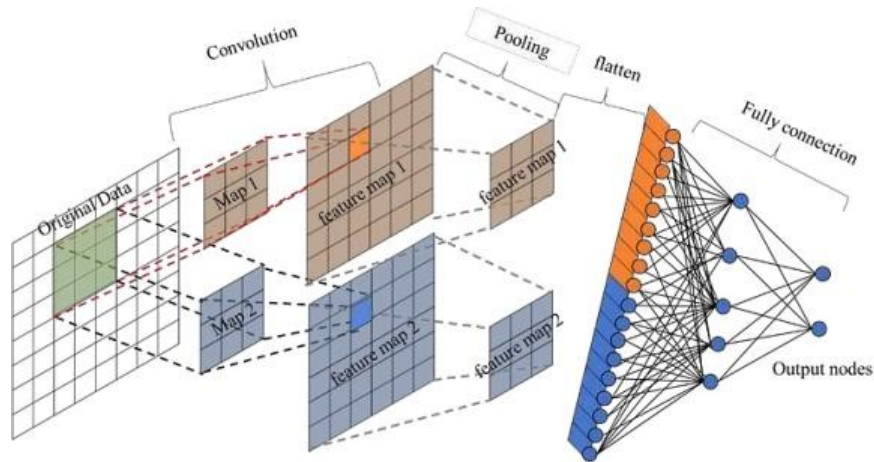


Figure 5: Structure of a Convolutional Neural Network (Zhao and Cai, 2017)

(b) Transformer

The Transformer model (Figure 6), introduced by Vaswani et al. (2017), is a deep learning architecture based on the self-attention mechanism. Initially designed for natural language processing (NLP), it overcomes the long-term dependency issues of traditional RNNs and LSTMs while offering significant improvements in computational efficiency through parallelization. Transformers are now widely adopted in speech recognition, computer vision, and multimodal applications. Their core concepts include:

- **Self-Attention:** Enables weighted interactions across all positions in a sequence to capture dependencies.
- **Multi-Head Attention:** Learns multiple representation subspaces by applying self-attention multiple times, then integrates outputs through linear transformation.
- **Positional Encoding:** Provides sequential order information to the model. In this study, temporal encoding is used to preserve time-series characteristics.
- **Residual Connections & Layer Normalization:** Enhance gradient stability and training convergence.
- **Full Parallelism:** Replaces sequential RNN computation with parallelized operations for faster training.

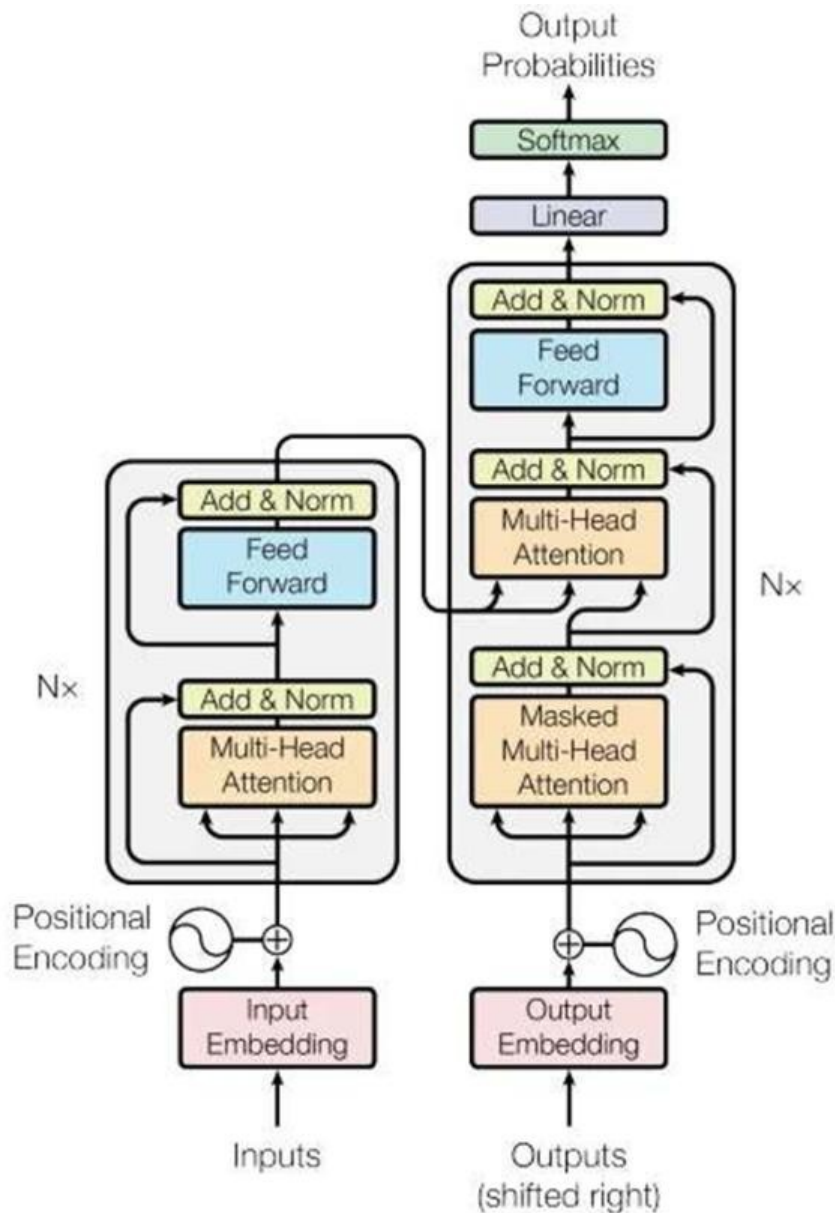


Figure 6: Structure of the Transformer model (Vaswani et al., 2017)

Section 2. Integration of CNN and Transformer

Recent advances highlight the complementary strengths of CNNs and Transformers. CNNs excel in local feature extraction from structured spatial data, while Transformers capture long-range dependencies, such as temporal dynamics. Their integration provides a hybrid framework well-suited for residual landslide analysis (Figure 7):

- **CNN:** Extracts localized spatial features such as textural patterns in imagery.
- **Transformer:** Models global dependencies and sequential characteristics via self-attention.

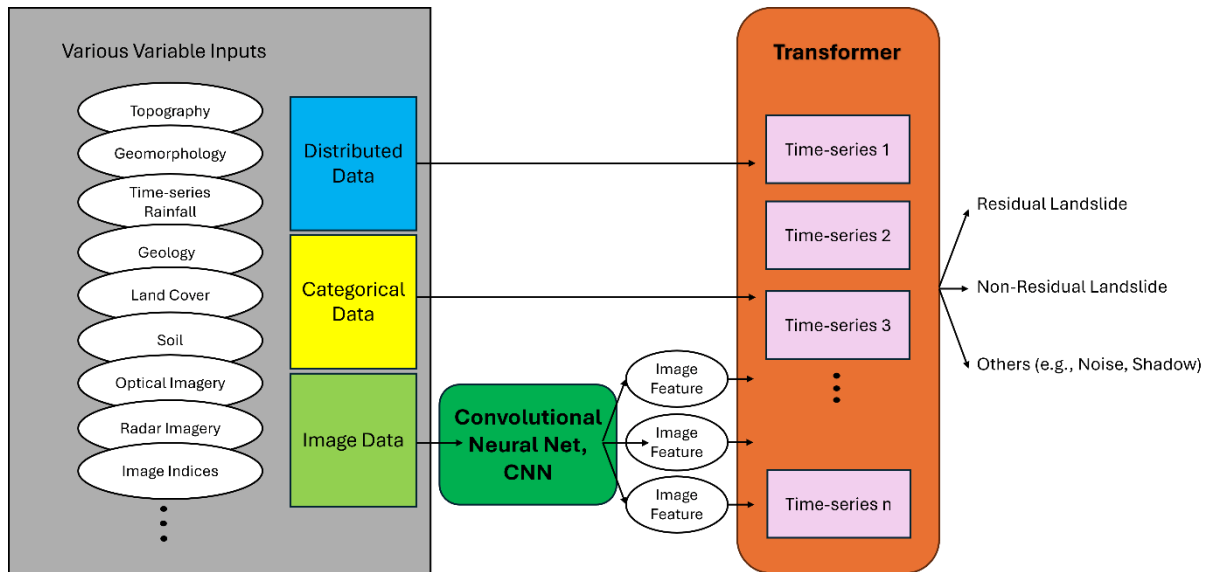


Figure 7: Integration of CNN and Transformer in this study

The model inputs include distributed data (topography, rainfall, soil, and land cover) and multi-temporal satellite imagery. CNN layers first extract spatial features from imagery, which are then processed by Transformer modules to capture temporal dependencies. The final model outputs classify residual landslide conditions into categories such as residual landslide, non-residual landslide, and activity levels. Shadowed areas or unclassified land covers are excluded as “no-data” zones.

This hybrid design enables the model to simultaneously leverage spatial and temporal information, thereby improving the capacity to characterize slope dynamics and enhancing residual landslide potential (activity) analysis.

Section 3. Model Application and Evaluation

The experimental area was divided into sub-watersheds to define training, testing, and validation datasets for the residual landslide inventory. Residual landslides with varying activity levels were used as samples, with 70% allocated for training and 30% for testing. To minimize data-split bias and improve model robustness, the random sampling process was repeated 100 times with independent training–testing splits.

Model performance was assessed using the following evaluation metrics:

- **Accuracy** = $(TP + TN) / (TP + TN + FP + FN)$: Overall correct classification rate; less sensitive to class imbalance.
- **Precision (P)** = $TP / (TP + FP)$: Proportion of correctly predicted positives, important in high-cost misclassification scenarios.

- **Recall (R)** = $TP / (TP + FN)$: Proportion of actual positives correctly predicted, critical for avoiding omission errors.

Where TP = True Positive, TN = True Negative, FP = False Positive, and FN = False Negative.

Finally, the results of residual landslide potential analysis were cross-validated with multi-temporal satellite imagery and the SWCA residual landslide inventory to confirm the reliability and practical applicability of the developed AI model.

Research Data

In order to optimize the effectiveness of model analysis, the study divided the experimental area into multiple spatial units based on sub-watersheds. Considering the respective advantages of Convolutional Neural Networks (CNN) and Transformer models, key influencing factors such as satellite image features, elevation, geology, and rainfall were categorized into two groups for organization and statistical analysis at the sub-watershed level:

CNN was applied to extract image indices (e.g., NDVI) and other single-image features from satellite imagery. For non-image data such as elevation and slope, which are static spatial factors (Table 3), CNN-based feature extraction was not applied.

Transformer was employed to capture the temporal variations of multi-temporal satellite features and dynamic factors such as rainfall (Table 4).

Through this design, a comprehensive model for potential assessment was established, followed by validation of its predictive performance.

Table 3: Static data applied in the model

Data Type	Description	Data Source
Topography	Elevation, slope, aspect, curvature	Derived from 5 m Digital Elevation Model (DEM), Department of Land Administration, Ministry of the Interior
Hydrology	Stream Power Index (SPI), Topographic Wetness Index (TWI), drainage density	Same as above

Data Type	Description	Data Source
Geology	Lithology, soil distribution	Central Geological Survey, Ministry of Economic Affairs (NCDR Datahub)

Table 4: Multi-temporal data applied in the model

Data Type	Description	Data Source
Rainfall Observation Data (2008– 2023)	2.5 km climate gridded monthly dataset	Central Weather Administration, CODiS Climate Data Service (https://codis.cwa.gov.tw/)
Sentinel-2 (2016–2024)	Surface reflectance imagery, NDVI index, WLSI index	European Space Agency (ESA) (https://browser.dataspace.copernicus.eu/)
Event-based Landslide Inventory (2008–2023)	Vector polygon dataset	Soil and Water Conservation Bureau, BigGIS (https://gis.ardswc.gov.tw/map)

Section 1. Sub-watershed Delineation

o establish a model suitable for the study area, the region was divided into sub-watersheds based on terrain elevation and river discharge. The delineation aimed to ensure that each sub-watershed contained sufficient representative data (e.g., slope, aspect, curvature; grid count > 30) to reflect local characteristics. Additionally, each residual landslide was assigned to a single sub-watershed, while maintaining the integrity of individual residual landslide units and avoiding fragmentation across multiple sub-watersheds (original residual landslide count: 168).

Sub-watersheds were generated using different flow accumulation thresholds of 20 ha, 40 ha, 80 ha, 100 ha, 200 ha, and 400 ha (Figure 8). The number of residual landslide units fragmented under each threshold was then counted (Table 5).

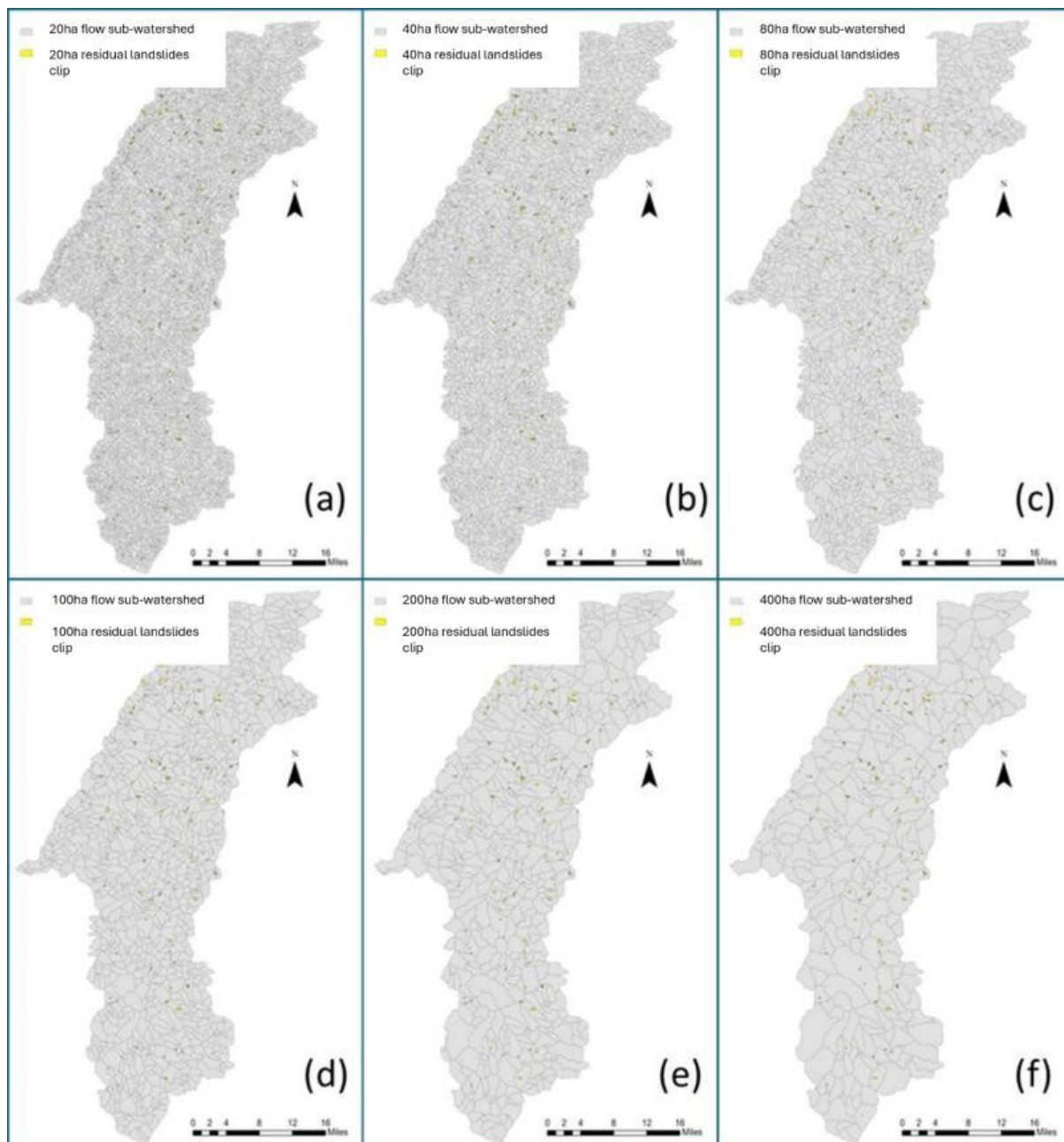


Figure 8: Sub-watersheds delineated using different flow accumulation thresholds

(a) 20 ha, (b) 40 ha, (c) 80 ha, (d) 100 ha, (e) 200 ha, (f) 400 ha

Table 5: Residual Landslides fragmentation under different flow accumulation thresholds

Flow Accumulation Threshold	Number of Sub-watersheds	Number of Residual Landslides
20 ha	8,253	306
40 ha	3,878	243

Flow Accumulation Threshold	Number of Sub-watersheds	Number of Residual Landslides
80 ha	1,882	184
100 ha	1,469	177
200 ha	695	150
400 ha	356	116

The study ultimately selected 100 ha as the threshold for delineating sub-watersheds. This value preserved the integrity of over 80% of residual landslide units while ensuring sufficient representativeness of topographic parameters and statistical analyses. Figure 9 presents the distribution of sub-watershed areas, showing that approximately 95% of the units are smaller than 450 ha.

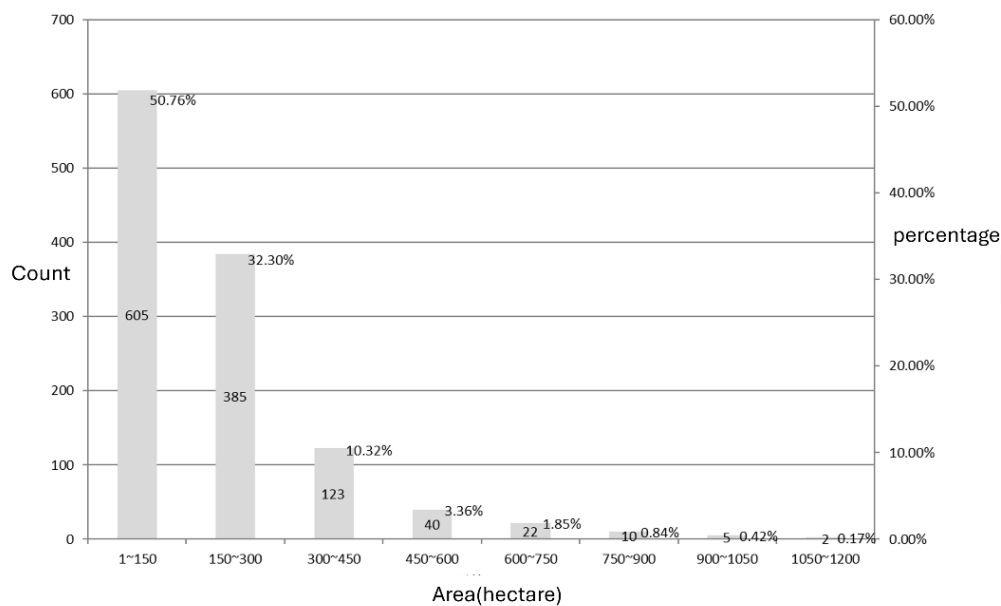


Figure 9: Sub-watershed area distribution in the study region

Section 2. Residual Landslide Data

Residual landslide data formed the basis of model training. Each residual landslide was first assigned to the corresponding sub-watershed based on spatial location. For cases where a residual landslide spanned multiple watersheds, the unit was assigned to the watershed

containing the largest portion of its area. After assignment, the number, area, volume, and activity status of residual landslides within each sub-watershed were compiled.

Since the existing residual landslide database lacks precise formation dates, spatial overlay analysis was conducted with the landslide event inventory. The earliest event year overlapping the residual landslide footprint was defined as its earliest collapse year. Years of subsequent collapses were also recorded as references for temporal analysis. For residual landslides without corresponding records in the inventory, it was inferred that such units either predated the study's observation period or were not directly formed by identifiable disaster events.

Section 3. Satellite Imagery

This study primarily utilized Sentinel-2 **Surface Reflectance (SR)** imagery to calculate spectral indices. Sentinel-2 consists of Sentinel-2A (launched June 23, 2015) and Sentinel-2B (launched March 7, 2017). Each satellite has a 10-day revisit cycle.

The sensors record **Top-Of-Atmosphere (TOA) Reflectance**, which includes both **Surface Reflectance (SR)** and **atmospheric effects**. The latter result from scattering and absorption by atmospheric gases and aerosols (e.g., dust, water droplets, ice crystals), which distort the true spectral properties of surface objects. These distortions affect analytical accuracy.

To address this issue, this study used **Sentinel-2 Level-2A products**, which apply atmospheric correction to restore surface reflectance. Such products enhance the ability to distinguish bare soil, vegetation, and surrounding environments in landslide areas, and improve the accuracy of vegetation, water, and soil indices—facilitating reliable change detection across temporal imagery.

Benefiting from Sentinel-2's ~290 km swath width and standardized 100 × 100 km tiling system, and since the entire study area is contained within a single tile (51QTF: 51Q denotes UTM zone, TF represents MGRS 100 km grid), only this tile was selected for analysis. This approach ensured geometric and radiometric consistency, simplified processing, and avoided errors from mosaicking multiple tiles.

The study collected all Sentinel-2 Level-2A imagery from **2016 to 2024**, merging the 10 m and 20 m resolution bands (10 bands total; Table 6) to allow direct extraction of the required bands for further analysis.

Table 6: Sentinel-2A band configuration

SENTINEL-2 Bands	Central Wavelength (μm)	Resolution (m)
Band 1 – Coastal aerosol	0.443	60
Band 2 – Blue	0.490	10
Band 3 – Green	0.560	10
Band 4 – Red	0.665	10
Band 5 – Vegetation Red Edge	0.705	20
Band 6 – Vegetation Red Edge	0.740	20
Band 7 – Vegetation Red Edge	0.783	20
Band 8 – NIR	0.842	10
Band 8A –Vegetation Red Edge	0.865	20
Band 9 – Water vapor	0.945	60
Band 10 – SWIR - Cirrus	1.375	60
Band 11 – SWIR	1.610	20
Band 12 – SWIR	2.190	20

(Data Source: ESA, www.esa.int/Applications/Observing_the_Earth/Copernicus/SENTINEL-2)

Given the mountainous setting of the study area, steep terrain often produces extensive shadows, hindering the detection of subtle surface features such as residual landslide boundaries and unstable sediments. Ideally, images captured under the highest solar elevation angle (near local noon) would minimize shadows. However, Sentinel-2, operating on a sun-synchronous orbit, passes Taiwan at approximately 10:30 AM daily, preventing acquisition of true-noon imagery. Solar elevation also varies seasonally, reaching its maximum in mid-June to early July when the study area is nearly under direct solar incidence.

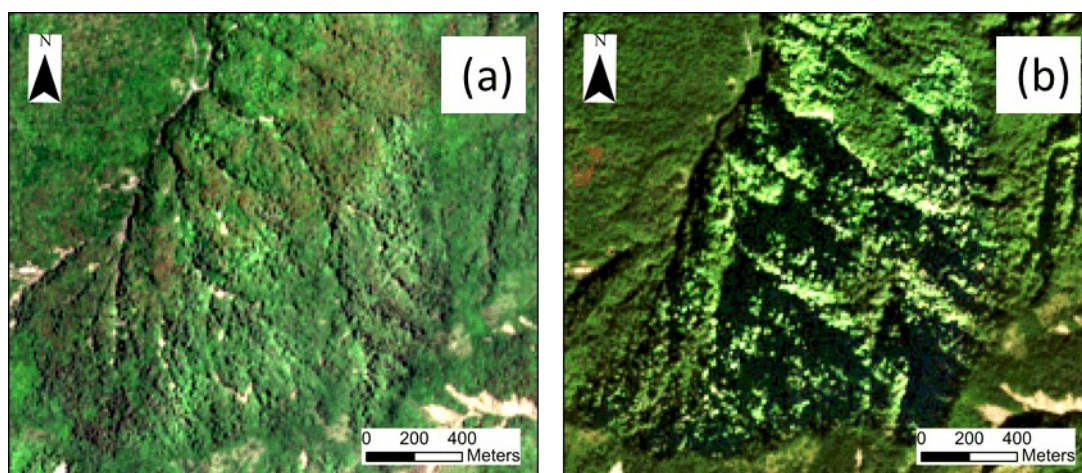


Figure 10: Shadow effects in Sentinel-2 mountain imagery
(a) June 24, 2023, (b) December 11, 2023)

To minimize shadow interference, this study selected imagery acquired only between April and September each year, when solar elevation is relatively high. Figure 11 presents the imagery selected for analysis: from 2016 to 2024, a total of 29 images were chosen, averaging 2 images per year. The first two years (2016–2017) had fewer acquisitions due to lower acquisition frequency, whereas from 2018 onward, approximately 72–73 acquisitions per year were available, of which 4–5 images per year met the selection criteria.

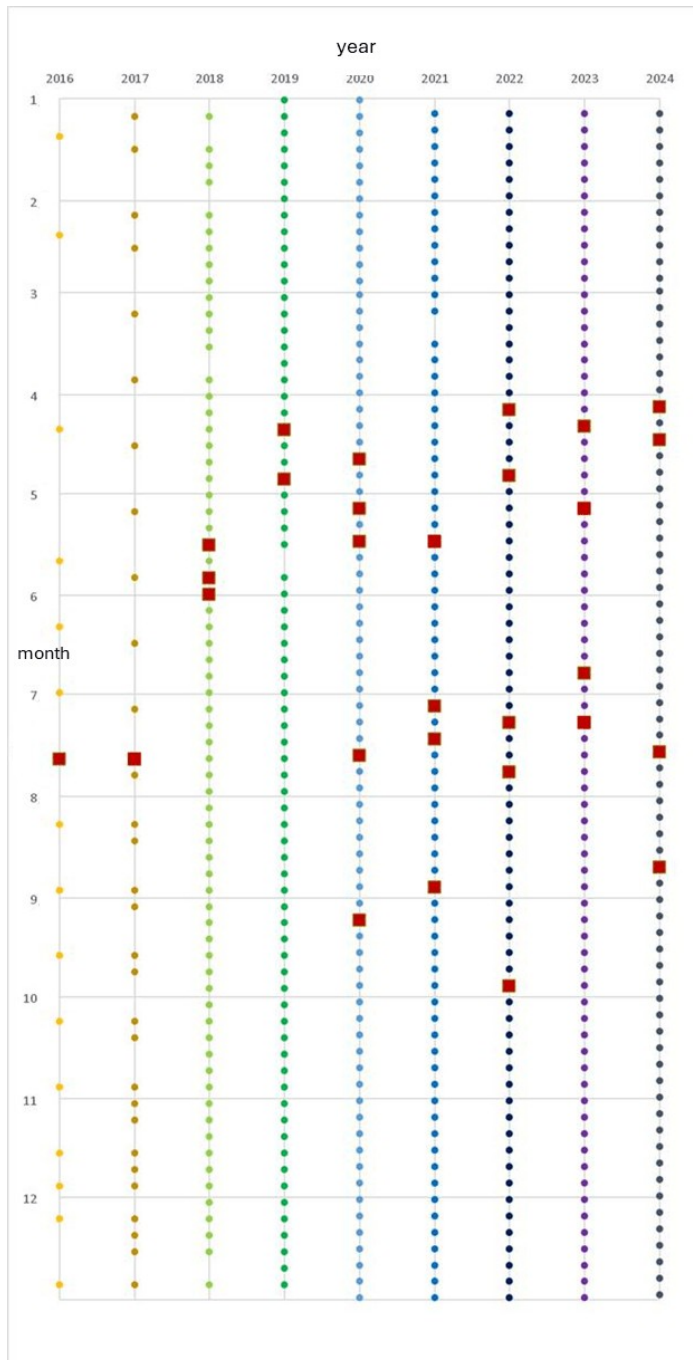


Figure 11: Sentinel-2 acquisition dates (dots) and selected images (squares) between 2016 and 2024

Results and Discussion

Section 1. Landslide Samples

The model was established using sub-watersheds as the sample unit (a total of 1,192 sub-watersheds). Only multi-temporal data incorporated the self-attention mechanism. Residual landslide data were used as learning samples, categorized into three hierarchical levels:

1. **Landslide vs. Non-Landslide:** Landslides refer to units where collapse occurred between 2008 and 2023; non-landslide units are those with no collapse during this period.
2. **Residual Landslide vs. Non-Residual Landslide:** Within the landslide data, units were further distinguished as residual landslides or non-residual landslides.
3. **Residual Landslide Activity Levels:** Residual landslides were classified into three activity levels: high, medium, and low.

Table 7 lists the sample counts for each category of landslide. Figure 12 shows the distribution of landslides and residual landslide activity levels across sub-watersheds.

Table 7: Sample counts for each landslide category

Category (Count)	Residual Landslide	Activity Level	Count
Landslide (998)	Residual Landslide (132)	High	30
		Medium	50
		Low	52
	Non-Residual Landslide		866
Non-Landslide (194)			194

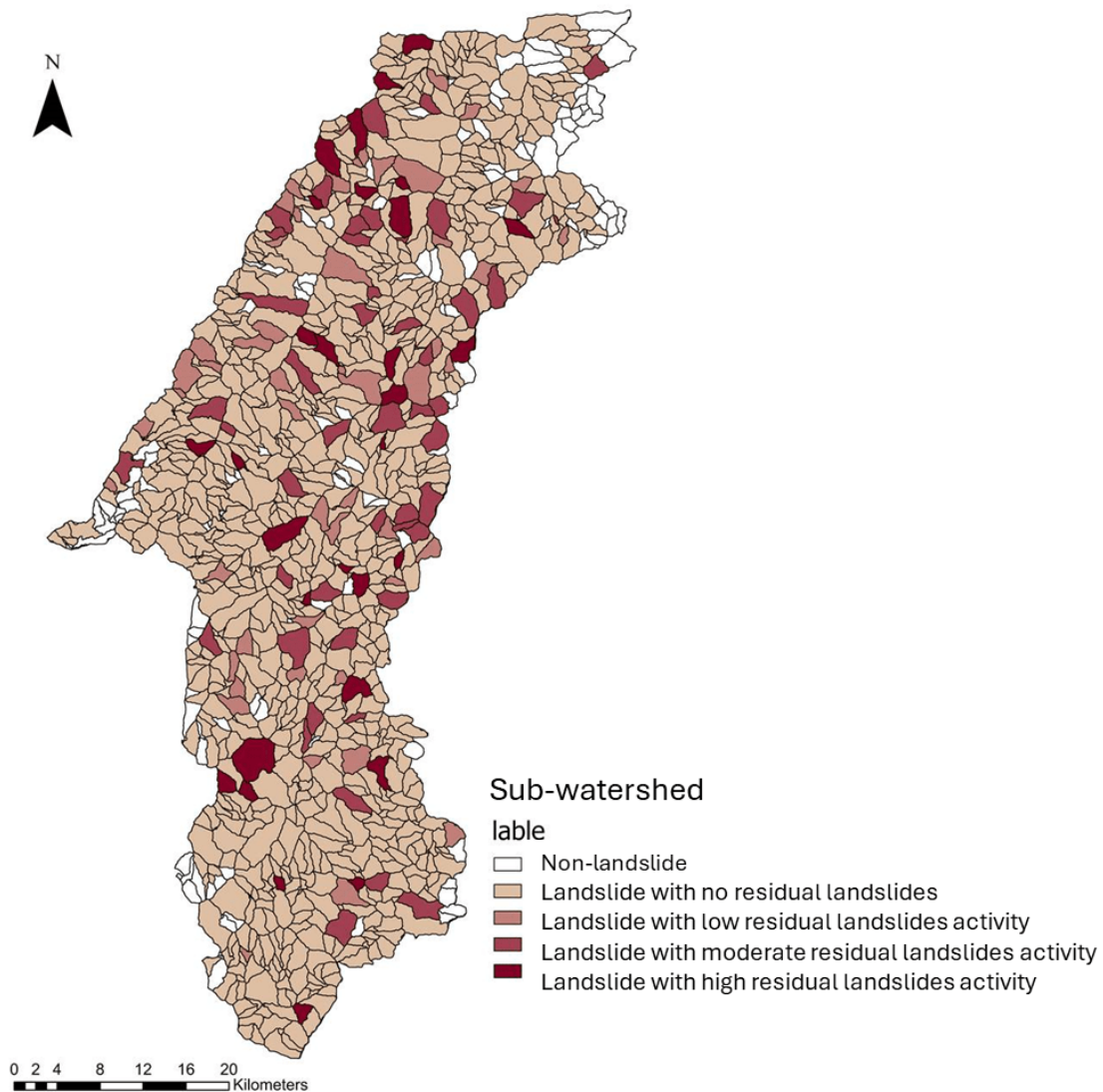


Figure 12: Distribution of landslides and residual landslide activity levels across sub-watersheds

Section 2. Model Parameter Setup

This study applied various parameters in the model, which can be classified into static data and multi-temporal dynamic data. The details of each parameter are as follows.

1. Static Data Description

Static data include terrain parameters derived from a Digital Elevation Model (DEM), such as elevation, slope, and aspect, as well as hydrological indices including Stream Power Index (SPI) and Topographic Wetness Index (TWI).

(1) Terrain Parameters

- **Elevation:** All elevation data in this study were derived from a 5 m resolution DEM.

- **Slope:** Slope values were calculated from the DEM using the Slope tool in ArcGIS Pro for the entire study area.
- **Aspect:** Aspect distribution was computed from the DEM using the Aspect tool in ArcGIS Pro. Since aspect is a circular variable, directly encoding it using linear values or dummy variables would disrupt its geographic continuity and gradual variation. To address this, trigonometric functions were used to convert the aspect angle (θ) into two independent continuous variables: one representing the north-south component (**Northness, $\cos(\theta)$**) and another representing the east-west component (**Eastness, $\sin(\theta)$**). This method preserves the circular geographic information of the original aspect while linearizing it, enabling effective integration into the potential assessment model.
- **Curvature:** Curvature involves second-order derivatives of elevation. To avoid abrupt fluctuations and anomalies caused by DEM noise and errors, the DEM was first smoothed using the Focal Statistics tool in ArcGIS Pro. Total curvature, plan curvature, and profile curvature were then calculated using the Curvature tool for the study area.

(2) Hydrological Parameters

- **Stream Power Index (SPI):** The Stream Power Index (SPI) is commonly used in river erosion and geomorphological change analyses. It reflects the erosive capacity of water flow at a given location, i.e., its ability to transport sediment and erode the surface. Higher SPI values indicate stronger erosive power. It is calculated as:

$$SPI = \ln (A_s \cdot \tan \beta) \text{-----} (1)$$
 where A_s is the **Specific Catchment Area**, representing the upstream catchment area per unit contour length, approximated by multiplying flow accumulation by cell size; β is the slope in degree.

β is the slope in degree.

- **Topographic Wetness Index (TWI):** The Topographic Wetness Index (TWI) quantifies the influence of topography on soil moisture. Steep slopes promote rapid water flow, reducing infiltration and potentially lowering soil moisture, whereas gentle slopes allow water to remain longer on the surface, increasing infiltration and soil moisture. It is computed as:

$$TWI = \ln \left(\frac{A_s}{\tan \beta} \right) \text{-----} (2)$$

where A_s is the Specific Catchment Area and β is the slope in degree.

- **River Density (D_s):** River density represents the total length of river channels per unit area and is often used to indicate terrain fragmentation or susceptibility to erosion. Generally, higher river density reflects more fragmented terrain and greater fluvial incision. It is calculated as:

$$D_s = \frac{L_T}{A} \text{-----}(3)$$

where L_T is the total length of rivers within the sub-watershed and A is the area of the sub-watershed.

2.Multi-Temporal Data Description

Dynamic data in this study were mainly derived from multi-temporal satellite imagery indices, rainfall, and historical landslide statistics. The details are as follows:

- **Weighted Landslide State Index (WLSI):** This study adopted the Weighted Landslide State Index (WLSI) proposed in the 112th-year Innovative Research Program of the Soil and Water Conservation Bureau: “*Application of Multi-Satellite Measurement Methods for Analyzing Terrain Changes and Stability Assessment of Landslide Slopes*”. WLSI has been validated for effectively distinguishing soil, colluvium, and bedrock on landslide slopes. The WLSI is calculated as:

$$WLSI = K_1 \cdot \frac{\text{Band 11} - \text{Band 2}}{\text{Band 11} + \text{Band 2}} + K_2 \cdot \frac{\text{Band 8} - \text{Band 4}}{\text{Band 8} + \text{Band 4}} \text{-----}(4)$$

The first term distinguishes colluvium from bedrock, with values ranging from -1 to 1 (Band11 = SWIR, Band2 = Blue). The second term is the NDVI, highlighting vegetation by the contrast between near-infrared (Band8) and red (Band4) reflectance, also ranging from -1 to 1. $NDVI < 0$ indicates bare ground or water, while $NDVI > 0.7$ indicates dense vegetation. K_1 and K_2 are weights for the colluvium-bedrock and NDVI components, summing to 1. For equal weights ($K_1 = K_2 = 0.5$), WLSI values classify surface types as: (1) water: < 0 ; (2) bedrock: $0 \sim 0.2$; (3) soil/colluvium: $0.2 \sim 0.5$; (4) vegetation: > 0.5 .

- **Temporal Landslide Data:** Annual landslide event data within the study area were aggregated at the sub-watershed level to compute yearly landslide area, landslide area ratio, and landslide frequency.
- **Physiographic Fragility (F_p):** According to the definitions from the Soil and Water Conservation Bureau research platform, physiographic fragility (F_p) is evaluated on a $1.3 \text{ km} \times 1.3 \text{ km}$ grid across Taiwan. Key indicators include the occurrence of new landslides per year and annual landslide area. For each year, the natural logarithm of cumulative new landslide area and frequency is computed. These values are averaged (μ) and standardized ($\pm\sigma$) to categorize each grid into five levels: low,

medium, medium-high, high, and very high. To calculate long-term landslide indicators at the sub-watershed level, area differences among sub-watersheds were considered. The cumulative new landslide area was divided by sub-watershed area before taking the natural logarithm, forming the sub-watershed physiographic fragility index.

- **Rainfall Data:** Monthly 2.5 km climate grid data from the Central Weather Bureau CODiS climate observation service were used. Two types of rainfall time series were established: (1) for each sub-watershed, the monthly maximum rainfall for 2008–2023; (2) monthly rainfall associated with specific landslide events based on the landslide event inventory.

Integrating all static and dynamic parameters, this study established **43 variables** for model application. Multi-temporal data were aggregated on an annual basis, and all variable definitions and data sources are summarized in Table 8.

Table 8: Variables Used in the Model Application

Data Source	Variable Name (Statistics per Sub-Watershed)	Description
Sub-watershed	shape_area	Sub-watershed area (ha)
Topographic Parameters – Elevation	dem_min	Minimum elevation
	dem_max	Maximum elevation
	dem_mean	Mean elevation
	dem_std	Standard deviation of elevation
Topographic Parameters – Slope	slope_min	Minimum slope
	slope_max	Maximum slope
	slope_mean	Mean slope
	slope_std	Standard deviation of slope
Topographic Parameters – Aspect	aspectcos_mean	Mean north-south component of aspect

Data Source	Variable Name (Statistics per Sub-Watershed)	Description
	aspectcos_std	Standard deviation of north-south component of aspect
	aspectsin_mean	Mean east-west component of aspect
	aspectsin_std	Standard deviation of east-west component of aspect
Topographic Parameters – Curvature	curvature_mean	Mean total curvature
	curvature_std	Standard deviation of total curvature
	curvatureprofile_mean	Mean profile curvature
	curvatureprofile_std	Standard deviation of profile curvature
	curvatureplan_mean	Mean plan curvature
	curvatureplan_std	Standard deviation of plan curvature
Hydrological Parameters – SPI	SPI_min	Minimum Stream Power Index
	SPI_max	Maximum Stream Power Index
	SPI_mean	Mean Stream Power Index
	SPI_std	Standard deviation of Stream Power Index
Hydrological Parameters – TWI	TWI_min	Minimum Topographic Wetness Index
	TWI_max	Maximum Topographic Wetness Index
	TWI_mean	Mean Topographic Wetness Index

Data Source	Variable Name (Statistics per Sub-Watershed)	Description
Hydrological Parameters – River Density	TWI_std	Standard deviation of Topographic Wetness Index
	river_length	Total river length
	river_density	River density
Sentinel-2 Satellite Imagery – WLSI	WLSI_min	Annual minimum WLSI
	WLSI_max	Annual maximum WLSI
	WLSI_mean	Annual mean WLSI
	WLSI_std	Annual standard deviation of WLSI
CWB CODiS Climate Observation Data – Rainfall	Rain_min	Annual minimum of maximum monthly rainfall
	Rain_max	Annual maximum of maximum monthly rainfall
	Rain_mean	Annual mean of maximum monthly rainfall
	Rain_std	Annual standard deviation of maximum monthly rainfall
Event-based Landslide Inventory – Multi-Temporal Landslide	ls_true	Annual occurrence of landslide (Yes/No)
	ls_frequency	Landslide occurrence frequency
	ls_area	Annual landslide area per sub-watershed
	ls_areapercent	Annual landslide area ratio per sub-watershed
	ls_fragility	Physiographic fragility

Data Source	Variable Name (Statistics per Sub-Watershed)	Description
	ls_rain	Rainfall corresponding to annual landslide events

Section 3 Preliminary Results

In the model application, the current study has integrated all variables except for multi-temporal satellite imagery. In the preliminary test, since multi-temporal imagery was not applied, the CNN-based image feature extraction component of the model was not used, and the model was primarily established based on the Transformer framework.

The study used 70% of the samples for model training and 30% for model validation. At present, two sets of preliminary results have been obtained:

1. Model classification predictions for landslide vs. non-landslide sub-watershed.
2. Model classification predictions for residual landslide vs. non-residual landslide sub-watershed.

First, for the landslide vs. non-landslide model classification prediction, although landslide sites occupy most of the samples in the study area, random sampling was used to establish training and validation datasets. A verification step was applied to ensure that no less than 10% of the samples were non-landslide sites, excluding parameters derived from the event-based landslide inventory (see Table 8). To ensure model stability, sampling and model prediction were repeated 100 times. The results of each trial (landslide: 1; non-landslide: 0) were averaged to obtain the expected probability of landslide occurrence for each sub-watershed. The results are shown in Figure 13.

Second, for the residual landslide vs. non-residual landslide model classification prediction, random sampling was similarly used to establish training and validation datasets. All variables listed in Table 8 were included. To ensure stability, the procedure was repeated 100 times, and the results of each trial (residual landslide: 1; non-residual landslide: 0) were averaged to obtain the expected probability of residual landslide occurrence for each sub-watershed. The results are shown in Figure 14.

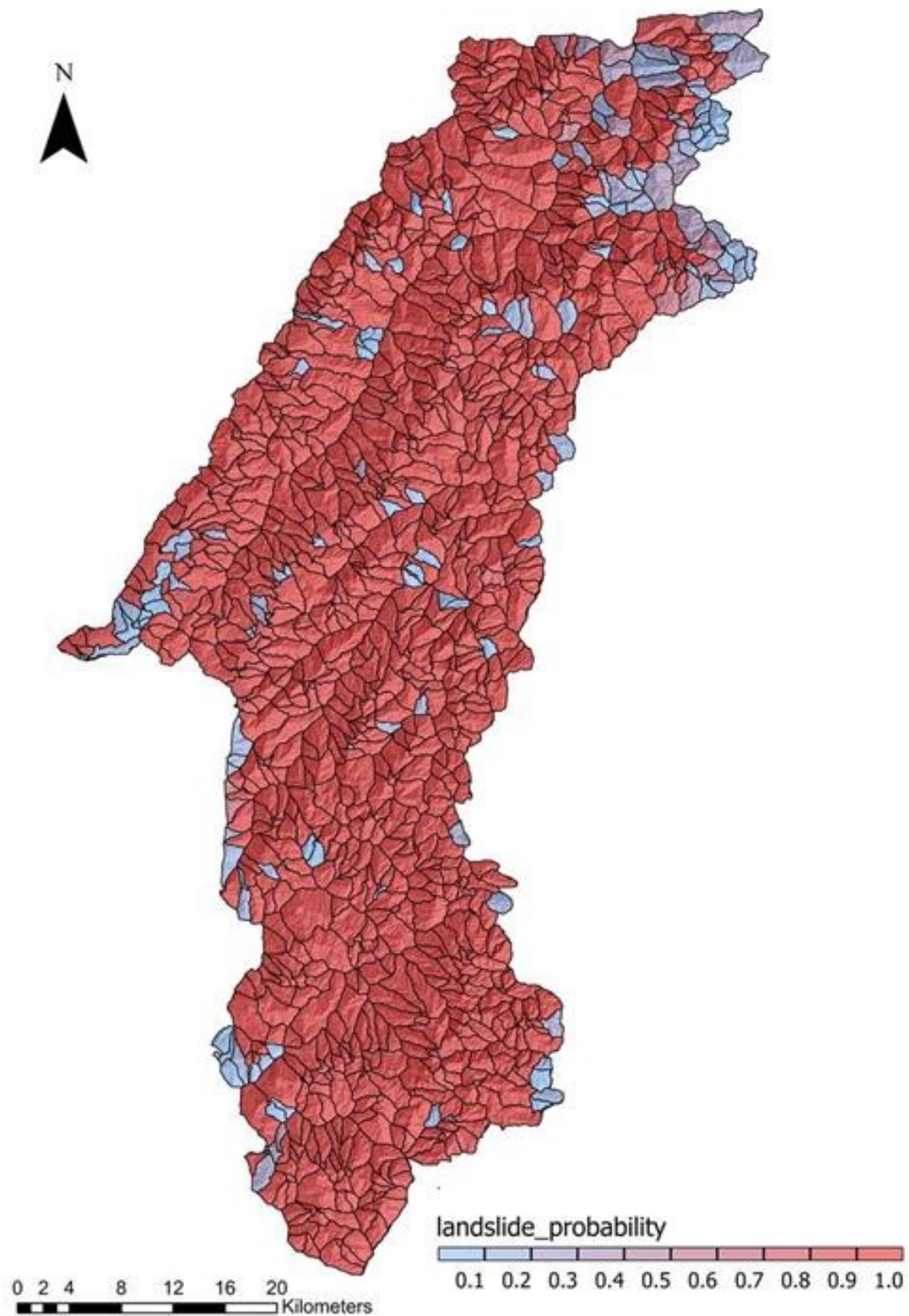


Figure 13: Model 1 landslide prediction results

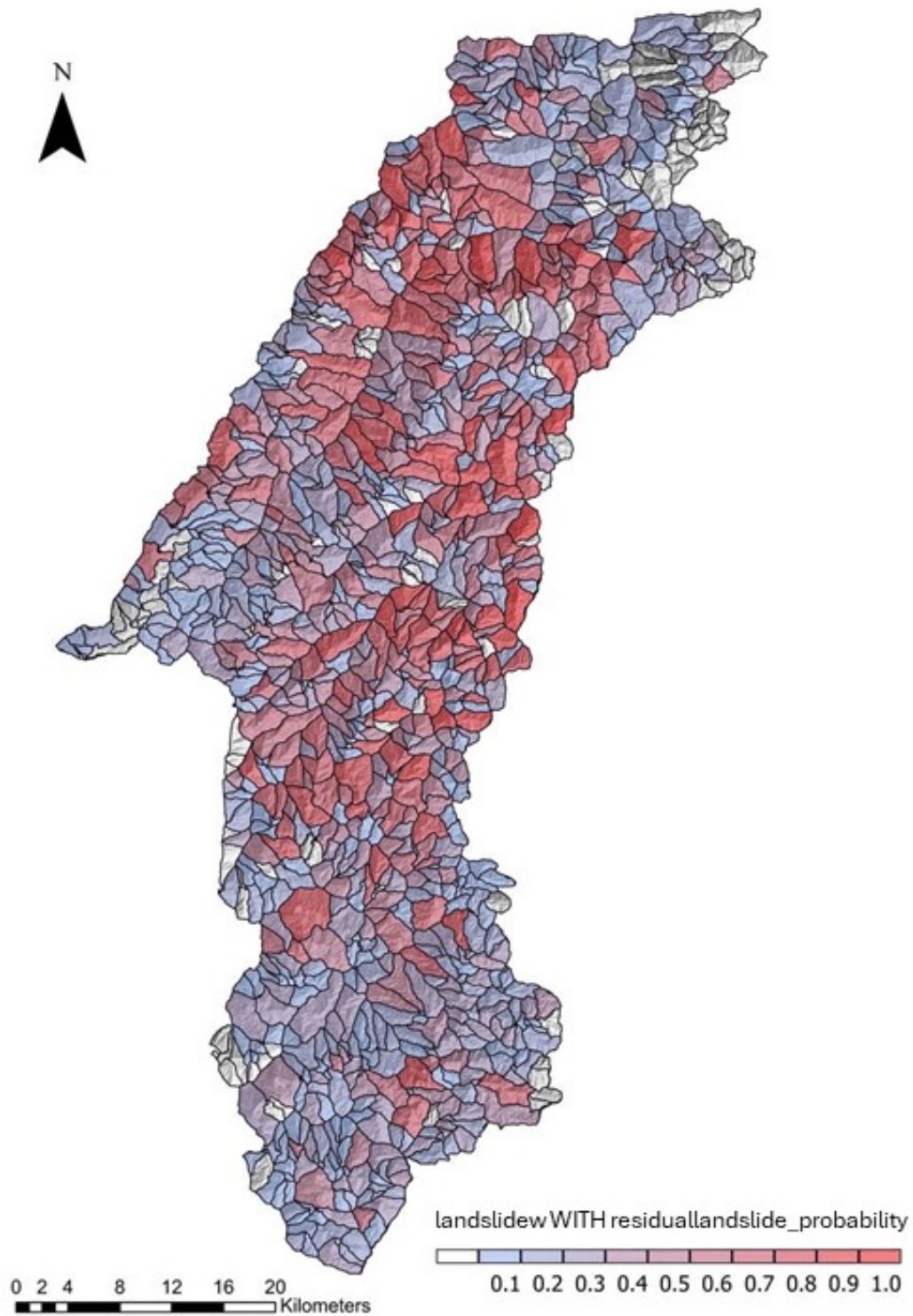


Figure 14: Model 2 residual landslide prediction results

Table 9: Preliminary Results of Model Testing

Model Prediction Target		Accuracy	Precision	Recall
1	Landslide / Non-landslide	0.96	0.92	0.94
2	Residual Landslide / Non-residual Landslide	0.82	0.80	0.77

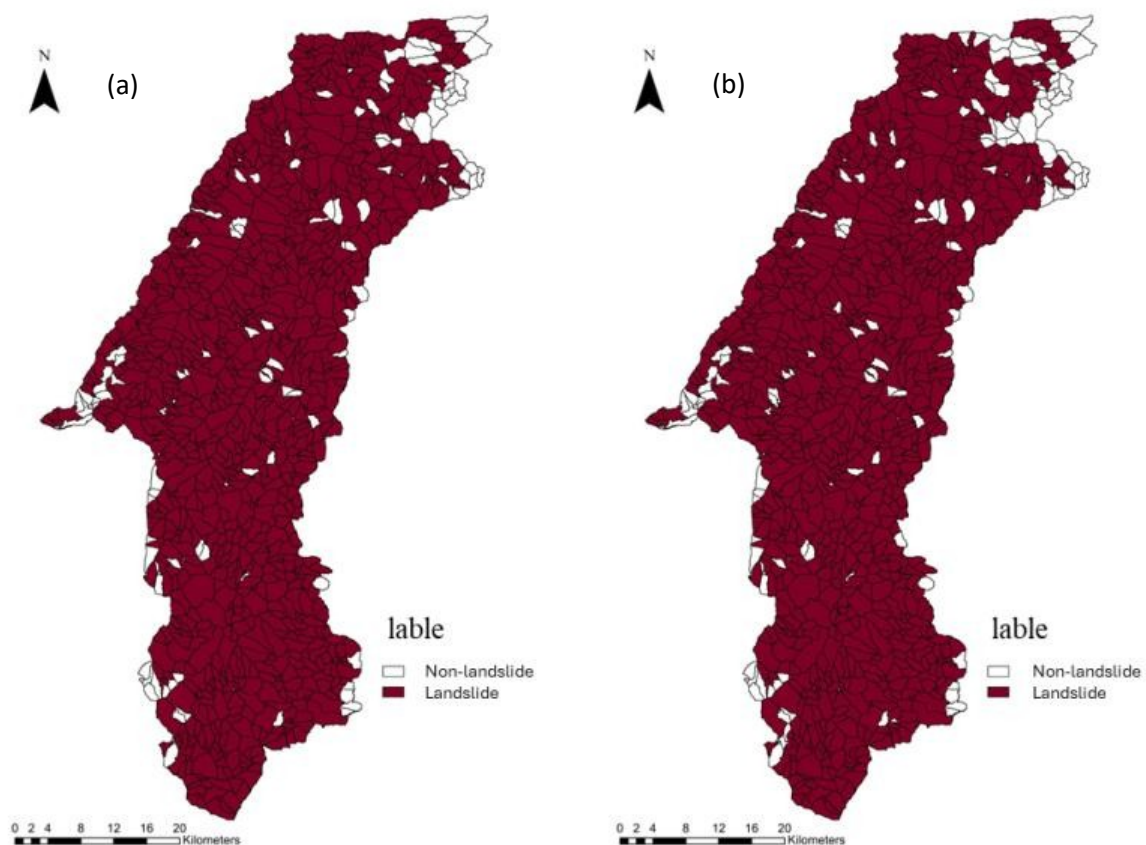


Figure 15: Model 1 landslide prediction results

(a) Observed landslide distribution, (b) Model-predicted landslide distribution

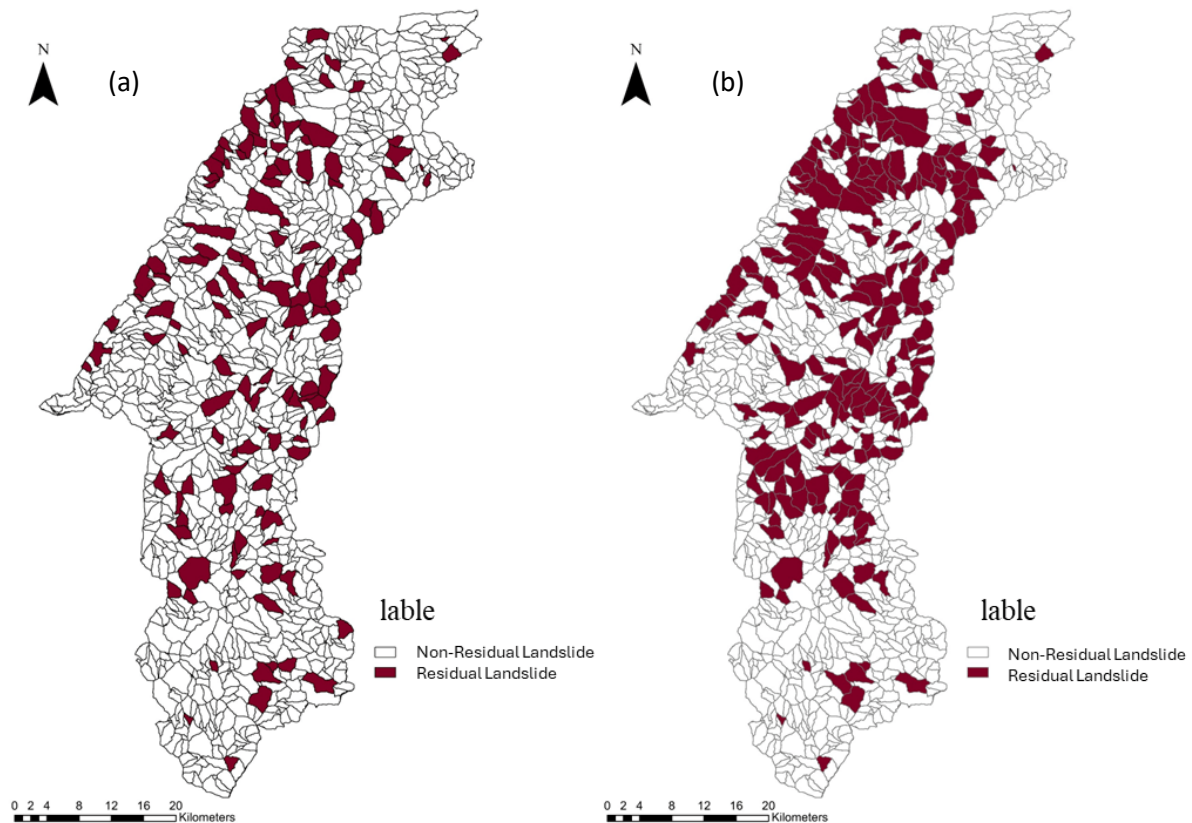


Figure 16: Model 2 residual landslide prediction results.
(a) Observed residual landslide distribution, (b) Model-predicted residual landslide distribution

Currently, the project has completed these two preliminary tests. For residual landslide prediction (Model 2), future work will integrate multi-temporal satellite imagery and incorporate CNN-based image feature analysis to improve prediction performance, and further establish models for predicting the activity levels of residual landslides.

Conclusion and Recommendation

For residual slope risk, this study aims to propose an artificial intelligence–based analytical approach that integrates Convolutional Neural Networks (CNN) and Transformer methods to construct a model for assessing the potential of residual slopes. The method can be applied to inventory residual slopes in mountainous areas and evaluate their activity.

At present, this study has completed the collection of relevant data for model application, integrating both dynamic and static parameters. A total of 43 parameters have been established as model variables, and two experiments have been conducted: (1) landslide prediction and (2) residual slope prediction. The results show that the landslide prediction

model achieved an accuracy as high as 0.96, while the residual slope prediction model also attained an accuracy of 0.82.

In the next stage, this study will integrate multi-temporal satellite imagery and incorporate CNN-based image feature analysis to further enhance the predictive capability of the model. Moreover, a predictive model for the activity of residual slopes will be developed, followed by an analysis of the model performance to assess the feasibility of applying this approach for residual slope inventory in mountainous regions of Taiwan. The ultimate goal is to provide valuable support for sediment disaster prevention and mitigation efforts.

References

1. Agriculture and Rural Development and Soil and Water Conservation Agency. (2024). Residual slope determination operation manual: 2024 revised edition. Agriculture and Rural Development and Soil and Water Conservation Agency.
2. Chuang, C.-Y., Chen, C.-Y., & Chan, W.-Y. (2024). Application of geomorphic vulnerability for establishing instability potential classification of watershed sediment. *Journal of Chinese Soil and Water Conservation*, 55(3), 122–130.
3. Agriculture and Rural Development and Soil and Water Conservation Agency. (n.d.). Technical research and development platform. Retrieved September 30, 2025, from <https://tech.ardswc.gov.tw/>
4. Vaswani, A., Shazeer, N., Parmar, N., Uszkoreit, J., Jones, L., Gomez, A. N., Kaiser, Ł., & Polosukhin, I. (2017). Attention is all you need. In *Advances in Neural Information Processing Systems*, 30. Curran Associates, Inc.
5. Zhao, T., & Cai, C. (2017). Deep learning in landslide detection: Using CNNs for feature extraction and recognition. *Landslides*, 14(2), 763–773. <https://doi.org/10.1007/s10346-016-0730-1>